Softening Coefficient of Reinforced Concrete Elements Subjected to Three-Dimensional Loads

Moheb Labib[1], Yashar Moslehy[2], and Ashraf Ayoub[3]

ABSTRACT

Reinforced concrete structures are prone to fail under the effect of complex three-dimensional loading conditions. Accurate constitutive models for concrete under the effect of triaxial stresses are therefore necessary in order to predict the proper response. Strong interaction between in-plane and out of plane shear loads has been observed in experimental tests of concrete structures. This paper presents the derivation of concrete constitutive laws under the effect of triaxial stresses, in particular the softening coefficient, using the results of large-scale tests on representative concrete panels. The experimental program of 7 full-scale panel specimens is briefly described, and the results are then used to derive analytical expressions for the softening coefficient under the effect of bi-directional shear. Finally, existing membrane shear theories are modified to take into consideration the effect of applied out-of-plane shear. The response of the tested panels proved to be accurately predicted using the new theory.

Key Words: Compressive strength, Cracks & cracking, Shear, Testing, structural elements, Testing, apparatus & methods

[1] Louis Berger International, Dallas, TX, USA
[2] Energo Engineering, Houston, TX, USA
[3] City, University of London, London, UK

INTRODUCTION

The behavior of many complex structures such as curved beams, spiral stairs, plate structures such as slabs and foundation mats, and shell structures such as domes, oil platforms, and nuclear containment structures as shown in Figure 1 requires knowledge of the constitutive laws of reinforced concrete elements subjected to a triaxial state of stress. Previous experimental tests of concrete specimens subjected to triaxial loads focused on the behavior under hydrostatic compression (e.g. Gerstle, 1981). Experimental evaluation of representative concrete specimens under the effect of combined triaxial tension/compression loads has not been fully explored. In particular, the effect of out-of-plane loads typically results in a different crack pattern that will alter the main characteristics of the concrete material. As a result, the softening behavior of concrete under triaxial loading and other constitutive parameters will change. There exists a need to revise current models of concrete structures subjected to three-dimensional loads.

RESEARCH SIGNIFICANCE

The purpose of this work is to develop appropriate material parameters for concrete subjected to a triaxial state of stress, in particular the softening coefficient. Such parameters were not properly derived in the literature, and are needed for accurate prediction of the behavior of complex three-dimensional reinforced concrete structures. The softening coefficient greatly affects the behavior of concrete structures; and while it has been extensively evaluated for two-dimensional stresses, no information exists for its value in the case of three-dimensional state of stress. This research attempts to fill this gap in the literature by proposing new functions for the concrete softening coefficient in the case of three-dimensional loads. To conduct this task, large-scale reinforced concrete panel specimens are tested at the University of Houston Universal Panel Tester under the effect of in-plane and varying out-of-plane loads. The results are used to

improve existing shear theories to account for the effect of out-of-plane loads. It is expected that the newly-developed concrete material properties will enhance the accuracy of model simulation of complex reinforced concrete structures.

MODELING OF RC ELEMENTS UNDER A 3D STATE OF STRESS

Vecchio and Selby (1991) presented an analysis of reinforced concrete 3D solids. The constitutive relations implemented in the formulation are relations extrapolated from two-dimensional models and based on the modified compression field theory. The same constitutive laws used in evaluating the membrane shear were adopted for concrete in the direction of the largest principle compressive and tensile strain. They used the same previous constitutive relationships for the intermediate principle direction whether it is in compression or tension. The researchers reported that more work is required to refine and verify the accuracy of the three-dimensional formulation especially in the absence of a complete three-dimensional model for concrete.

Mullapudi and Ayoub (2013) used Vecchio and Selby's model in the formulation of shear fiber element to predict the behavior of different structural members subjected to complex loadings. The values of the concrete uni-axial strains in principal directions 1, 2, and 3 have eight conditions, and the strength in one direction is affected by the strain state in the other directions. Adebar et al. (1989) developed a model to consider the interaction between membrane shear and transverse shear. The combination of transverse and membrane shear involves tri-axial strains. Adebar proposed to consider biaxial strains over the thickness of the section, but tri-axial strains are considered at one reference plane (usually the section mid-plane or the plane at the centroid of the flexural tension reinforcement). The influence of tri-axial strains on the biaxial strains stresses is assumed to be uniform over the thickness and is accounted for by a set of membrane

force corrections ΔN_x, ΔN_y, and ΔN_{xy}. Adebar proposed an equation for the crack check considering the reinforcement to be aligned in 3 directions. The tri-axial relationship is a generalization of the biaxial relationship in the Modified compression field theory.

Maekawa et al. (1996) proposed the strain decomposition and stress recomposition. The 3D strain field is decomposed into three in-plane sub-spaces. In each sub-space, the component stresses are computed using the 2D crack model and constitutive laws. All component stresses on the decomposed sub-spaces are re-composed again to form the three-dimensional stress field. An orthogonal co-ordinate system is set up so that the principal axis (1) is normal to the initially introduced crack plane and the remaining axes (2 and 3) are located within the reference plane. Here three 2D sub-spaces designated by axes (1,2), (2,3), and (1,3) can be defined. The first crack is seen in the (1,2) and (1,3) planes, while plane (2,3) contains no cracks at this moment because it coincides with the plane of the first crack itself. Any further crack is treated in the 2D sub-spaces, based on the initial crack.

Marti (1990) proposed a design method for slabs subjected to combined membrane and transverse shear by satisfying equilibrium without consideration of deformation. In this model, the slabs were divided into two top and bottom covers in addition to a concrete core. The model assumes that the covers will carry moments and membrane forces, while the transverse shear is assigned to the core. A limit for the nominal shear stress due to the principle shear force has been suggested that differentiates between uncracked and cracked core areas. For the case of uncracked core, no transverse reinforcement has to be provided and the in-plane reinforcement must not be strengthened to account for transverse shear. For diagonally cracked core areas, a truss-model-based design procedure has been developed that permits the dimensioning of the necessary transverse and in-plane reinforcements.

MEMBRANE SHEAR SOFTENED TRUSS MODEL

Several models for in-plane shear in concrete elements that were based on the smeared-crack approach were developed in the past three decades. In these models, the equilibrium equations assume the stresses in the concrete struts and steel bars to be smeared. Similarly, the strains of steel and concrete are also smeared, and are obtained by averaging the strains along a steel bar that crosses several cracks. The constitutive laws of concrete and steel bars were developed through large-scale panel testing, and relate the smeared stresses to the smeared strains of the element (Belarbi and Hsu 1994, 1995; Hsu and Zhang 1996). The first work to develop such constitutive laws was the one by Vecchio and Collins (1981), who proposed the compression field theory (CFT) to predict the nonlinear behavior of cracked reinforced concrete membrane elements. The CFT, however, was unable to take into account the tension-stiffening effect of the concrete. The researchers later improved their model and developed the modified compression field theory (MCFT) (Vecchio and Collins 1986), in which the tension stiffening of concrete was accounted for by imposing a concrete tensile stress across the shear crack. At the University of Houston, Belarbi and Hsu (1994, 1995) and Pang and Hsu (1995) used a different approach and developed the rotating-angle softened-truss model (RA-STM). In this model, the tension-stiffening effect of concrete was taken into account. Later, the UH research group improved their work and developed the fixed-angle softened-truss model (FA-STM) (Pang and Hsu 1996; Hsu and Zhang 1997; Zhang and Hsu 1998). This model is capable of predicting the concrete contribution to shear resistance by assuming a shear stress along the crack direction. Zhu et al. (2001) derived a rational shear modulus and developed a simple solution algorithm for the FA-STM. The work was further extended by determining the Hsu/Zhu ratios (Zhu and Hsu 2002) for Poisson effect. This led to the development of the softened membrane model (SMM), which can accurately predict the entire response of the specimen, including both the ascending

and the descending branches. While these pioneering models greatly enhanced the basic understanding of the in-plane shear behavior of RC elements, they cannot be directly implemented for the case of elements subjected to three-dimensional shear loads. The reason is that the three-dimensional loading condition greatly affects the crack pattern and the failure mode of the specimen. There is a need to expand the scope of smeared crack models to account for three-dimensional load effects. Before doing this, a brief review of previous work related to the behavior of reinforced concrete structures subjected to two-dimensional loading is presented as this will be expanded to account for three-dimensional effects.

In the past 20 years, Hsu and his colleagues performed over 130 panel tests using the Universal Panel Tester (Hsu et al. 1995) at the University of Houston. A series of three rational models for the monotonic shear behavior of reinforced concrete elements (panels) was developed. Figure 2 describes the stresses acting on the components of a reinforced concrete membrane element subjected to in-plane shear and normal stresses. The directions of the longitudinal and the transverse steel bars are designated as ℓ and t axes, respectively, constituting the $\ell - t$ coordinate system as shown in Figure 2 (a). The normal stresses are designated as σ_ℓ and σ_t in the ℓ and t directions, respectively, and the shear stresses are represented by $\tau_{\ell t}$ in the $\ell - t$ coordinate system. Based on the reinforced concrete sign convention for Mohr's circles, a positive shear stress $\tau_{\ell t}$ is the one that causes clockwise rotation of a reinforced concrete element (Hsu, 1993).

The applied principal stresses for the reinforced concrete element are defined as σ_2 and σ_1 based on the $2-1$ coordinate system as shown in Figure 2 (d). The angle between the direction of the applied principal compressive stress ($2-$axis) and the direction of the longitudinal steel ($\ell -$axis) is defined as the fixed-angle α_2, because this angle does not change

when the three in-plane stresses, σ_ℓ, σ_t, and $\tau_{\ell t}$, increase proportionally. This angle α_2 is also called the steel bar angle because it defines the direction of the steel bars with respect to the applied principal stresses. The principal stresses in concrete coincide with the applied principal stresses σ_1 and σ_2 before cracking. When the principal tensile stress σ_1 reaches the tensile strength of concrete, cracks will form and the concrete will be separated by the cracks into a series of concrete struts in 2 direction as shown in Figure 2 (f). If the element is reinforced with different amounts of steel in the ℓ and t directions, i.e., $\rho_\ell f_\ell \neq \rho_t f_t$ in Figure 2 (c), the direction of the principal stresses in concrete after cracking will deviate from the directions of the applied principal stresses. The new directions of the post-cracking principal stresses in concrete are defined by the $d-r$ coordinate system as shown in Figure 2 (e). Accordingly, the principal compressive stress and the principal tensile stress in the cracked concrete are defined as σ_d and σ_r, respectively.

The angle between the direction of the principal compressive stress in the cracked concrete ($d-$axis) and the direction of the longitudinal steel ($\ell-$axis) is defined as the rotating-angle α. The angle α is dependent on the relative amount of "smeared steel stresses," $\rho_\ell f_\ell$ and $\rho_t f_t$, in the longitudinal and the transverse directions as shown in Figure 2 (c). When $\rho_\ell f_\ell > \rho_t f_t$, the $d-r$ coordinate gradually rotates away from the $2-1$ coordinate and α becomes smaller with increasing load. With increasing applied proportional stresses (σ_ℓ, σ_t and $\tau_{\ell t}$), the deviation between the angle α and the angle α_2 increases. This deviation angle β is defined as $\alpha_2 - \alpha$. When the percentages of reinforcement are the same in the ℓ and t directions, the rotating angle α is equal to the fixed-angle α_2.

The fixed-angle softened-truss model (FA-STM) is based on the assumption that the direction of the cracks coincides with the direction of the applied principal compressive stress as shown in Figure 2 (f). In the fixed-angle softened-truss model, all equations are derived based on the fixed-angle α_2.

The three stress components σ_ℓ, σ_t, and $\tau_{\ell t}$ shown in Figure 2 (a) are the applied stresses on the reinforced concrete element viewed as a whole. The stresses on the concrete struts are denoted as σ_ℓ^c, σ_t^c, and $\tau_{\ell t}^c$ as shown in Figure 2 (b). The longitudinal and the transverse steel provide the smeared (average) stresses of $\rho_\ell f_\ell$ and $\rho_t f_t$ as shown in Figure 2 (c). The reinforcement is assumed to take only axial stresses, neglecting any possible dowel action. Summing the concrete stresses and the steel stresses in the $\ell-$ and the $t-$ directions and maintaining the equilibrium of forces and moments give the following equations:

$$\sigma_\ell = \sigma_\ell^c + \rho_\ell f_\ell, \quad (1)$$

$$\sigma_t = \sigma_t^c + \rho_t f_t, \quad (2)$$

$$\tau_{\ell t} = \tau_{\ell t}^c. \quad (3)$$

Equations 1-3 are the basic equilibrium equations for both RA-STM and FA-STM. When the three concrete stresses (σ_ℓ^c, σ_t^c, and $\tau_{\ell t}^c$) in the $\ell - t$ coordinate are transformed to the principal $d-r$ coordinate of concrete as in Figure 2 (g), we obtain the RA-STM. When the three concrete stresses (σ_ℓ^c, σ_t^c, and $\tau_{\ell t}^c$) are transformed to the principal 2-1 coordinate of the applied stresses as in Figure 2 (f), we obtain the FA-STM.

Equilibrium and Compatibility Equations

In the fixed-angle softened-truss membrane shear model (FA-STM), the direction of cracks is defined by the fixed angle α_2 in the principal 2-1 coordinate of the applied stresses. The three

equilibrium equations are obtained from Eqs. 1 to 3 by expressing the concrete stresses (σ_ℓ^c, σ_t^c, and $\tau_{\ell t}^c$) in terms of concrete stresses (σ_2^c, σ_1^c and τ_{21}^c) in the principal 2-1 direction through transformation (Pang and Hsu, 1996):

$$\sigma_\ell = \sigma_2^c \cos^2\alpha_2 + \sigma_1^c \sin^2\alpha_2 + \tau_{21}^c 2\sin\alpha_2\cos\alpha_2 + \rho_\ell f_\ell, \quad 4$$

$$\sigma_t = \sigma_2^c \sin^2\alpha_2 + \sigma_1^c \cos^2\alpha_2 - \tau_{21}^c 2\sin\alpha_2\cos\alpha_2 + \rho_t f_t, \quad 5$$

$$\tau_{\ell t} = (-\sigma_2^c + \sigma_1^c)\sin\alpha_2\cos\alpha_2 + \tau_{21}^c(\cos^2\alpha_2 - \sin^2\alpha_2), \quad 6$$

where

σ_1^c, σ_2^c = smeared (average) stresses of concrete in 1 and 2 directions, respectively,

τ_{21}^c = smeared (average) shear stress of concrete in $2-1$ coordinate, and

α_2 = angle of applied principal compressive stress ($2-$axis) with respect to longitudinal steel bars ($\ell-$axis).

The three compatibility equations, which represent the relationship through transformation between the strains (ε_ℓ, ε_t, and $\gamma_{\ell t}$) in the $\ell - t$ coordinate of the reinforcement and the strains ($\varepsilon_1, \varepsilon_2$, and γ_{21}) in the $2-1$ coordinate of the applied principal stresses, are expressed as follows (Pang and Hsu, 1996):

$$\varepsilon_\ell = \varepsilon_2 \cos^2\alpha_2 + \varepsilon_1 \sin^2\alpha_2 + \frac{\gamma_{21}}{2} 2\sin\alpha_2\cos\alpha_2, \quad 7$$

$$\varepsilon_t = \varepsilon_2 \sin^2\alpha_2 + \varepsilon_1 \cos^2\alpha_2 - \frac{\gamma_{21}}{2} 2\sin\alpha_2\cos\alpha_2, \quad 8$$

$$\frac{\gamma_{\ell t}}{2} = (-\varepsilon_2 + \varepsilon_1)\sin\alpha_2\cos\alpha_2 + \frac{\gamma_{21}}{2}(\cos^2\alpha_2 - \sin^2\alpha_2), \quad 9$$

where

ε_2, ε_1 = smeared (average) strains in $2-1$ directions, respectively, and

γ_{21} = smeared (average) shear strain in 2-1 coordinate.

Constitutive Relationship of Cracked Concrete in Compression

The softened compressive stress-strain relationship of concrete is established in the 2-1 coordinate as follows (Zhang and Hsu, 1998):

$$\sigma_2^c = \zeta f_c' \left[2\left(\frac{\varepsilon_2}{\zeta\varepsilon_0}\right) - \left(\frac{\varepsilon_2}{\zeta\varepsilon_0}\right)^2 \right], \qquad \frac{\varepsilon_2}{\zeta\varepsilon_0} \le 1, \tag{10}$$

or

$$\sigma_2^c = \zeta f_c' \left[1 - \left(\frac{\varepsilon_2/\zeta\varepsilon_0 - 1}{4/\zeta - 1}\right)^2 \right], \qquad \frac{\varepsilon_2}{\zeta\varepsilon_0} > 1, \tag{11}$$

where

$$\zeta = \left(\frac{5.8}{\sqrt{f_c'}} \le 0.9\right)\left(\frac{1}{\sqrt{1+400\bar{\varepsilon}_1}}\right)\left(1 - \frac{|\beta|}{24^\circ}\right), \tag{12}$$

Constitutive Relationship of Cracked Concrete in Tension

The tensile stress-strain relationship of concrete in the $2-1$ coordinate is given as follows (Belarbi and Hsu, 1994):

$$\sigma_1 = E_c \varepsilon_1, \qquad \varepsilon_1 \le \varepsilon_{cr}, \tag{13}$$

or

$$\sigma_1 = f_{cr}\left(\frac{\varepsilon_{cr}}{\varepsilon_1}\right)^{0.4}, \qquad \varepsilon_1 > \varepsilon_{cr}, \tag{14}$$

where

E_c = elastic modulus of concrete taken as $3875\sqrt{f_c'}$ (f_c' and $\sqrt{f_c'}$ are in MPa),

ε_{cr} = concrete cracking strain taken as 0.00008, and

f_{cr} = concrete cracking stress taken as $0.31\sqrt{f_c'}$ (f_c' and $\sqrt{f_c'}$ are in MPa).

Constitutive Relationship of Steel Bars Embedded in Cracked Concrete

The smeared (average) tensile stress-strain relationship of steel embedded in concrete in the $\ell - t$ coordinate, can be expressed as follows:

$$f_s = E_s \bar{\varepsilon}_s, \qquad \bar{\varepsilon}_s \le \bar{\varepsilon}_n, \tag{15}$$

$$f_s = f_y\left[(0.91-2B)+(0.02+0.25B)\frac{\bar{\varepsilon}_s}{\varepsilon_y}\right], \qquad \bar{\varepsilon}_s > \bar{\varepsilon}_n, \tag{16}$$

$$f_s = f_p - E_s(\bar{\varepsilon}_p - \bar{\varepsilon}_s), \qquad \bar{\varepsilon}_s < \bar{\varepsilon}_p, \tag{17}$$

$$\bar{\varepsilon}_n = \varepsilon_y(0.93-2B), \tag{18}$$

$$B = \frac{1}{\rho}\left(\frac{f_{cr}}{f_y}\right)^{1.5} \tag{19}$$

In the above equations, ℓ replaces *s* in the subscript of symbols for the longitudinal steel, and *t* replaces *s* for the transverse steel.

Constitutive Relationship of Cracked Concrete in Shear

Zhu et al. (2001) showed that the relationship between the shear stress and the shear strain of cracked concrete in the $2-1$ coordinate system could be rationally derived from the equilibrium equations and the compatibility equations by assuming that the direction of principal stresses coincides with the direction of principal strains. The new constitutive law of concrete in shear is given as:

$$\tau_{21}^c = \frac{\sigma_1^c - \sigma_2^c}{2(\varepsilon_1 - \varepsilon_2)}\gamma_{21} \tag{20}$$

While the previously described pioneering models greatly enhanced the basic understanding of the in-plane shear behavior of RC elements, they cannot be directly implemented for the case of elements subjected to bi-directional shear loads. The main goal of this paper is to improve the constitutive laws of concrete subjected to three-dimensional loads through additional panel testing. For this purpose, the capabilities of the UH panel tester were extended by installing an additional 10 two-way hydraulic cylinders in the out-of-plane direction as shown in Fig. 3. These Ten cylinders were applied at the top and bottom of an out-of-plane

steel frame connected to the panel tester, and the other 10 on its side. The hydraulic jacks were mounted on the panel tester and fixed to the steel frame with structural bolts with a diameter of 1 in. (25 mm). Upon installation of the jacks, they were connected to hydraulic lines. The installation of the out-of-plane hydraulic cylinders greatly enhanced the capabilities of the panel tester, which can now be used to test reinforced concrete elements subjected to a tri-directional state of stress. The next section briefly presents the results of the experimental tests. More details are given in Labib et al. (2013).

EXPERIMENTAL RESULTS

In total, eight reinforced concrete specimens were tested under the effect of bi-directional shear stresses. One of the specimens, OP0, was subjected to pure in-plane shear while another, OPR, was subjected to pure out-of-plane shear till failure. The other six specimens, denoted OP1-OP6, were subjected to a varying amount of out-of-plane shear loads of 13%, 22%, 28%, 52%, 72%, 82% of the shear capacity respectively, before an in-plane shear load was applied until failure. The specimens were all 55" (1400 mm) square with a web thickness of 7" (178 mm). The reinforcement arrangement was selected to represent the reinforcement grid in a typical shear wall. All specimens had two layers of #6 reinforcing bars inclined with a 45 degree angle. Specimens OP1, OP2 and OP3 were rectangular in shape. Specimens OP4, OP5 and OP6 had an I-cross sectional shape with a thicker edge of 16” (406 mm) and additional vertical reinforcement in order to resist larger out of plane loads, as shown in Figures 4 and 5. Specimen OPR also had an I-cross sectional shape, but its reinforcement was all in the vertical direction, since it was subjected to a pure out of plane load, as shown in Fig. 6. Further, to resist the out of plane shear load, closed stirrups across the width of the panels were required. These closed stirrups were substituted by U-shaped reinforcement bars for the case of inclined in-plane

reinforcement. The specimens were instrumented by 4 vertical, 4 horizontal and 2 diagonal Linear variable Differential Transducers (LVDTs) on each face of the panel. The material and geometric properties of all panels are given in Table 1.

To apply an out-of-plane shear load, first the south bottom and north top jacks apply a compressive load on the panel, while the south top and north bottom jacks apply a tensile load of the same magnitude. This will create two equal end moments acting at the edges of the panel. To equilibrate these moments, the out-of-plane jacks need to react with forces at the top and bottom of the specimen. To account for the associated end moments resulting from the application of the out-of-plane shear, the specimens had thicker edges where they were provided with additional flexural reinforcement, as discussed earlier. Once the out-of-plane loads are applied, an in-plane shear load is subsequently superimposed. This is performed by applying equal amounts of tensile and compressive stresses in the horizontal and vertical principal directions of the panel respectively.

The in-plane shear stress-strain relationship of all panels is shown in Figure 7, and the experimental results are presented in Table 1. The results reveal a strong effect of the out of plane load on the in-plane shear strength

INCORPORATING TRANSVERSE SHEAR IN MEMBRANCE SHEAR THEORY

The reduction in the strength of the membrane shear element when applying transverse shear affected the constitutive law of the concrete model. Using the same equilibrium and compatibility equations for the 2D membrane element, transverse shear can be related to the softening of the compression strut in the membrane shear theory. As we mentioned earlier, applying transverse shear reduced the membrane shear capacity for the panels. This reduction in the strength can be modeled as an extra softening effect for the compression strut of the

membrane shear element. To evaluate the value of softening coefficient in the case of bi-directional shear loads, the following procedure is followed:

The softening coefficient is the ratio between the compressive stresses in the concrete strut and the cylinder compressive concrete strength. The compressive stresses in the concrete strut were calculated as follow:

$$\sigma_{strut} = 2\tau - \sigma_{tension} \quad 21$$

The tensile strength of concrete was evaluated based on the previously mentioned tensile stress- strain relationship. The softening coefficient for the OP series panels is presented in Table 2 for the different out of plane shear loads.

The same procedure was followed by Pang (Pang and Hsu, 1995), and the specimens' material properties and calculated softening coefficients are summarized in Table 3 for the case of in-plane loading only. Belarbi (Belarbi and Hsu, 1995) used a different approach, where the softening coefficients were calculated as the ratio between maximum applied vertical compressive stresses on the panel to the cylinder compressive strength of the concrete. The material properties of their specimens and the corresponding softening coefficients are shown in Table 4. The softening coefficient for the OP series, Belarbi's, and Pang's panels are all shown in Figure 8 as a function of the applied lateral strain.

The softening coefficient for the OP series was less than that of the Pang's and Belarbi's panels. The panels with higher out-of-plane shear had lower softening coefficient. The difference between the softening coefficient for each panel in the OP series and that predicted by equation 12 is summarized in Table 5. The difference can be considered as a reduction in the softening coefficient due to the application of out-of-plane shear. Using least-square fitting, a mathematical expression for the ratio between the new and original softening coefficient is proposed as follow:

$$f(x) = 1 - \left(0.0178\,x - \frac{x^2}{10000} \right) \quad \text{Where } x = \frac{\tau_\circ}{\tau_{ou}} \times 100 \qquad 22$$

Figure 9 shows the experimental and mathematically-derived relation between the percentage of applied transverse shear and reduction factor of the softening coefficient. The correlation between the experimental data and mathematical model has an R^2 = 0.909. This slightly lower value is due to the fact that the correlation is not very accurate for high levels of out of plane loads. The complete expression for the softening coefficient including the effect of the concrete compressive strength, the lateral tensile strain, deviation between fixed and rotating angle and finally the effect of out-of-plane shear will therefore be:

$$\zeta = \left(\frac{5.8}{\sqrt{f_c^{'}}} \le 0.9 \right) \left(\frac{1}{\sqrt{1 + 400\,\varepsilon_1}} \right) \left(1 - \frac{|\beta|}{24^\circ} \right) \left(1 - \left(0.0178\,x - \frac{x^2}{10000} \right) \right) \qquad 23$$

Figure 10 shows the softening coefficient versus the applied lateral tensile strain at different levels of out-of-plane shear load. At a specific lateral tensile strain, it can be seen that increasing the applied out-of-plane shear caused a reduction in the softening coefficient, which will result in reducing the compressive strength of the compression strut. The out-of-plane shear stresses did not change or affect the constitutive laws for concrete in tension or those of the mild steel embedded in concrete.

Based on the above relationships, a solution algorithm (Figure 11) was then implemented to predict the strength of elements subjected to combination of in-plane and out-of-plane shear, where the ratio between out-of-plane shear to the maximum capacity of the element in the out-of-plane direction has to be specified. The membrane shear response for the OP series panels was predicted using the aforementioned algorithm. Figures 12 to 17 show the shear stress-strain prediction of the model to the behavior of the panels. The model was able to predict accurately the ultimate strength for most of the panels. The model overestimated the strength of specimen

OP6 and underestimated the strength of panel OP5. This can be attributed to the lack of accuracy of the mathematical model for high values of out of plane loads. In addition, for Panel OP5, the experimentally measured concrete strength was 8.92 ksi (61.5 MPa), which is 27% higher than the average concrete strength of other panels for which the mathematical equation was calibrated; this can justify the relatively lower accuracy of the model. Panel OP6 was subjected to a pure out-of-plane shear load without any in-plane compressive vertical loads, which resulted in the opening of flexural cracks along the specimen. These cracks further weakened the specimen, and hence the model was not able to accurately describe its behavior.

EFFECT OF IN-PLANE SHEAR REINFORCEMENT

Figure 18 shows the softening coefficient for different panels with different reinforcement ratios subjected to varying amounts of out-of-plane shear stresses and calculated using the aforementioned relationships. It can be noticed that the panels with lower reinforcement ratio achieved lower softening coefficient at higher lateral tensile strain. However, panels with higher reinforcement ratio achieved higher softening coefficient at lower lateral tensile strain. Figure 19 shows the stress-strain diagram for the panels with different in-plane shear reinforcement. The considered in-plane shear reinforcement ratios are 1%, 1.7%, and 2.5%. The panel with 1% reinforcement ratio was subjected to three different ratios of out-of-plane shear stresses which were 20%, 50%, and 90%. The panels with reinforcement ratios of 1.7% and 2.5% were subjected to one level of out-of-plane shear ratio which was 20% and 90%, respectively. The panels with 1% in-plane shear reinforcement had the steel yielding first followed by crushing of the concrete. Applying 20% of the out-of-plane shear load did not change the failure mode; yielding of steel observed first followed by concrete crushing. Applying 50% and 90% of the out-of-plane maximum capacity had the concrete crush before yielding of the steel. For panels with in-plane reinforcement ratios of 1.7% and 2.5%, applying the out-of-plane shear had the

concrete crushing before yielding of steel. Panels with 1% and 2.5% in-plane shear reinforcement and subjected to 90% of the out-of-plane shear ratio had almost the same capacity, which gives indication that at higher out-of-plane shear strength, the ratio of in-plane shear reinforcement is not significant. Figure 20 shows the interaction diagram between in-plane and out-of-plane shear strength for an element with different in-plane shear reinforcement ratio. From the figure, strong interaction is observed for panels with high in-plane shear reinforcement.

SUMMARY AND CONCLUSIONS

This paper aims at developing constitutive relations for RC elements subjected to bi-directional shear loads. Test results of 7 full scale reinforced concrete elements subjected to different combination of in-plane and out-of-plane loads are presented. The results showed clear interaction between applied in-plane shear and out-of-plane shear stresses. From the experimental data, a new expression for the softening coefficient in the presence of out of plane shear was developed. The effect of applying out-of-plane shear was then included in the membrane shear theories by modifying the softening coefficient of the compression strut. There was no observed change in the constitutive laws for concrete in tension or for the mild steel embedded in concrete. The model was able to capture the behavior of the tested panels rather accurately. Finally, the effect of the in-plane shear reinforcement ratio on the interaction diagram between in-plane and out of plane shear load capacity was investigated.

ACKNOWLEDGMENTS

The authors would like to express their deepest gratitude to Prof. T.T.C. Hsu and Prof. Y.L. Mo at the University of Houston for their guidance and advice regarding the use and extension of the Universal Panel Tester.

REFERENCES

Adebar, E. A. 1989. "Shear Design of Concrete Offshore Structures" PhD dissertation, University of Toronto, 428 pp.

Belarbi, A., and Hsu, T. T. C., 1994, "Constitutive Laws of Concrete in Tension and Reinforcing Bars Stiffened by Concrete," ACI Structural Journal, V. 91, No. 4, pp. 465-474.

Belarbi, A., and Hsu, T. T. C., 1995, "Constitutive Laws of Softened Concrete in Biaxial Tension-Compression,"

Gertsle, K. 1981. "Simple Formulation of Triaxial Concrete Behavior", ACI Structural Journal, 78(5): 382-387.

Hsu, T. T. C, Unified Theory of Reinforced Concrete, CRC Press, Inc., Boca Raton, FL, 336 pp, 1993.

Hsu, T. T. C., and Zhang, L. X., 1996, "Tension Stiffening in Reinforced Concrete Membrane Elements," ACI

Hsu, T. T. C., and Zhang, L. X., 1997, "Nonlinear Analysis of Membrane Elements by Fixed-Angle Softened-Truss Model," ACI Structural Journal, V. 94, No. 5, pp. 483-492.

Hsu, T. T. C.; Belarbi, A.; and Pang. X. B. 1995. "Universal Panel Tester," Journal of Testing and Evaluations, ASTM, V. 23, No. 1, pp. 41-49.

Labib, M., Moslehy, Y., and Ayoub, A.S. 2013. "Evaluation of the Constitutive Behavior of Reinforced Concrete Membrane Elements subjected to Bi-directional Shear Loads", ACI Structural Journal, 110(6): 1033-1044.

Maekawa, K., Pimanmas, A., and Okamura, H. "Nonlinear mechanics of Cocnrete" London, New York, Spon Press, (2003)

Marti, P. 1990. "Design of Concrete Slabs for Transverse Shear", ACI Structural Journal, V. 87, No. 2, pp. 180-190.

Mullapudi, T.R., and Ayoub, A.S. 2013. "Analysis of Reinforced Concrete Columns Subjected to Combined Axial, Flexure, Shear and Torsional Loads", Journal of Structural Engineering, ASCE, 139(4): 548-560.

Pang, X. B., and Hsu, T. T. C., 1995, "Behavior of Reinforced Concrete Membrane Elements in Shear," ACI Structural Journal, V. 92, No. 6, pp. 665-679.

Pang, X. B., and Hsu, T. T. C., 1996, "Fixed-Angle Softened-Truss Model for Reinforced Concrete," ACI Structural Journal, V. 93, No. 2, pp. 197-207.

Vecchio F. J. and Selby R. G., (1991) "Toward compression Field analysis of reinforced concrete solids" Journal of structural engineering, vol. 117, No. 6.

Vecchio, F. J., and Collins, M. P., 1986, "The Modified Compression Field Theory for Reinforced Concrete Elements Subjected to Shear," ACI Structural Journal, V. 83, No. 2, Mar.-Apr., pp. 219-231.

Vecchio, F., and Collins, M. P., 1981, "Stress-Strain Characteristic of Reinforced Concrete in Pure Shear," IABSE Colloquium, Advanced Mechanics of Reinforced Concrete, Delft, Final

Report, International Association of Bridge and Structural Engineering, Zurich, Switzerland, pp. 221-225.

Zhang, L. X., and Hsu, T. T. C., 1998, "Behavior and Analysis of 100 MPa Concrete Membrane Elements," ASCE Journal of Structural Engineering, V. 124, No. 1, pp. 24-34.

Zhu, R. H.; Hsu, T. T. C.; and Lee, J. Y., 2001, "Rational Shear Modulus for Smeared Crack Analysis of Reinforced Concrete," ACI Structural Journal, V. 98, No. 4, pp. 443-450.

Zhu, R. R. H., and Hsu, T. T. C., 2002, "Poisson Effect of Reinforced Concrete Membrane Elements," ACI Structural Journal, V. 99, No. 5, pp. 631-640.

FIGURE CAPTION

Table 1: Summary of the results for OP series

Panels	**OP0**	**OP1**	**OP2**	**OP3**	**OP4**	**OP5**	**OP6**	**OPR**
Thickness mm (in.)	178 (7)	178 (7)	178 (7)	178 (7)	178 (7)	178 (7)	178 (7)	178 (7)
Concrete strength MPa (ksi)	48.3 (7)	49.9 (7.2)	40 (5.8)	42.3 (6.1)	54.7 (7.9)	61.5 (8.9)	54 (7.9)	52 (7.5)
Applied out-of-plane shear								
Max. applied in-plane jack force kN(kip)	0	53 (12)	80 (18)	107 (24)	222 (50)	329 (74)	351 (79)	386 (87)
Applied out-of-plane shear force kN(kip)	0	20 (4.6)	31 (6.9)	41 (9.1)	85 (19.1)	125 (28.2)	134 (30.1)	147 (33)
Applied out-of-plane shear stress MPa (psi) on the 90° position	0	0.43 (62.20)	0.64 (93.29)	0.86 (124.39)	1.8 (259.15)	2.6 (383.54)	2.8 (409.46)	3.1 (453.36)
Applied out-of-plane shear stress MPa (psi) on the 45° position	0	0.3 (43.98)	0.45 (65.97)	0.61 (87.96)	1.26 (183.25)	1.87 (271.21)	2.0 (289.53)	2.21 (320.57)
Applied in-plane shear								
Max. applied horizontal force kN (kip)	184 (41.43)	160 (35.92)	172 (38.78)	141 (31.66)	114 (25.71)	127 (28.66)	44 (9.81)	0
Max. applied vertical load kN (kip)	196 (44.21)	179 (40.29)	174 (39.19)	151 (33.92)	124 (27.85)	137 (30.75)	63 (14.2)	0
Corresponding Max. Horizontal strain	0.024153	0.0044	0.00858	0.00639	0.00465	0.00487	0.00044	0
Corresponding Max. Vertical strain	-0.00332	-0.00175	-0.00131	-0.00233	-0.00166	-0.00181	-0.0008	0
Applied in-plane shear stress MPa (ksi)	8 (1.165)	7.2 (1.037)	7.3 (1.055)	6.1 (0.886)	5.0 (0.729)	5.6 (0.808)	2.6 (0.37)	0
Normalized out-of-plane shear on the 45° position	0	0.043 (0.52)	0.072 (0.86)	0.093 (1.12)	0.171 (2.05)	0.238 (2.86)	0.271 (3.25)	0.332 (3.98)
Normalized out-of-plane shear on the 90° position	0	0.06 (0.72)	0.10 (1.20)	0.13 (1.56)	0.24 (2.88)	0.34 (4.08)	0.38 (4.56)	0.47 (5.64)
Normalized in-plane shear	1.18 (29.97)	1.01 (12.12)	1.16 (13.92)	0.94 (11.28)	0.68 (8.16)	0.71 (8.52)	0.35 (4.2)	0

Table 2 Softening coefficient for OP series

Panels	$f_c^{'}$ (MPa)	ε_1 (mm/mm)	E_c (MPa)	f_{cr} (MPa)	σ_1 (MPa)	$(\tau_{lt})_{\exp}$ (MPa)	$(\sigma_2)_c$ (MPa)	$\zeta_{\exp}$	Out-of-plane (%)
OP0		0.01284						0.362	0
OP1	49.91	0.00812	33435	2.21	0.345	7.24	14.13	0.283	13
OP2	42.26	0.007664	30766	1.99	0.324	6.13	11.99	0.283	22
OP3	39.64	.005012	29797	1.93	0.372	7.31	14.27	0.36	28
OP4	54.67	0.002469	34993	2.27	0.586	5.10	9.65	0.176	46
OP5	61.49	0.002835	37113	2.41	0.586	7.51	14.54	0.236	68
OP6	54.25	0.002767	34860	2.27	0.558	3.45	6.27	0.116	72

Table 3 Softening coefficient for Pang (1991) panels

Panels	$f_c^{'}$ (MPa)	ε_1 (mm/mm)	E_c (MPa)	f_{cr} (MPa)	σ_1^c (MPa)	$(\tau_{lt})_{\exp}$ (MPa)	σ_2^c (MPa)	$(\sigma_2^c)_{\exp}$ (MPa)	$\zeta_{\exp}$
A1	42.19	0.05158	25348	1.99	0.151	2.275	4.398	2.351	0.104
A2	41.22	0.02676	25056	1.99	0.193	5.370	10.548	5.467	0.256
A3	41.64	0.01284	25182	1.99	0.262	7.659	15.056	7.914	0.362
A4	42.47	0.00634	25431	1.99	0.351	11.313	22.274	11.299	0.524
B1	45.22	0.02232	26243	2.07	0.220	3.964	7.707	3.998	0.170
B2	44.05	0.01413	25901	2.07	0.262	6.129	11.995	6.184	0.272
B3	44.88	0.01177	26143	2.07	0.282	4.357	8.431	4.453	0.188
B4	44.74	0.01030	26103	2.07	0.296	5.067	9.838	5.157	0.220
B5	42.81	0.00879	25534	2.07	0.310	7.156	14.001	7.190	0.327
B6	42.95	0.00837	25575	2.07	0.317	9.148	17.979	9.252	0.419
C2	41.5	0.03125	25140	1.99	0.186	0		7.321	0.264
C3	44.74	0.01215	26103	2.07	0.282	0		11.347	0.397
C4	41.98	0.00754	25286	1.99	0.324	0		9.196	0.448

Table 4: Softening coefficient for Belarbi (1991) Panels

Panels	$f_c^{'}$ (MPa)	σ_p,(MPa)	ε_1 (mm/mm)	$\zeta_{\exp}$
REF	44.6	34.87	0.00053	0.782
E0	38.2	33.56	0.00001	0.900
E1.5-1	44.57	28.34	0.00202	0.636
E1.5-1B	38.99	30.58	0.00289	0.784
E2-1	47.7	23.4	0.00431	0.491
E2'-1	39.58	29.88	0.00464	0.755
E2''-1*	41.24	27.13	0.00437	0.658
E2-1A	44.85	30.38	0.00316	0.677
E2-1B	38.31	21.98	0.00735	0.574
E4-1	40.56	20.78	0.00902	0.512
E4-.5	39.2	39.01	0.00865	0.468
E4-2	37.03	18.94	0.00970	0.511
E4-1A	37.3	20.49	0.00895	0.550
E10-1*	40.69	10.3	0.02764	0.253
E10-1A	36.88	12.9	0.02593	0.350
E10-1B	39.58	12.51	0.03708	0.316
R4-1*	41.98	33.26	0.00479	0.792
R10-1	39.04	20.85	0.00961	0.534
R30-1*	40.71	12.87	0.02933	0.316
F2*	40.11	11.85	0.02798	0.295
F3*	42.61	18.74	0.01433	0.440
F4*	41.89	20.85	0.00726	0.498

Table 5: Reduction in the softening coefficient for OP series due to application of out-of-plane shear

Panels	$f_c^{'}$ (MPa)	Out-of-plane (%)	ε_1 (mm/mm)	ς_{theor}	ζ_{exp}	Reduction Factor
OP0		0	0.012840	0.363	0.362	0.995
OP1	49.91	13	0.008120	0.437	0.283	0.649
OP2	42.26	22	0.007664	0.446	0.283	0.635
OP3	39.64	28	0.005012	0.519	0.360	0.692
OP4	54.67	46	0.002469	0.638	0.176	0.276
OP5	61.49	68	0.002835	0.616	0.236	0.383
OP6	54.25	72	0.002767	0.620	0.116	0.187

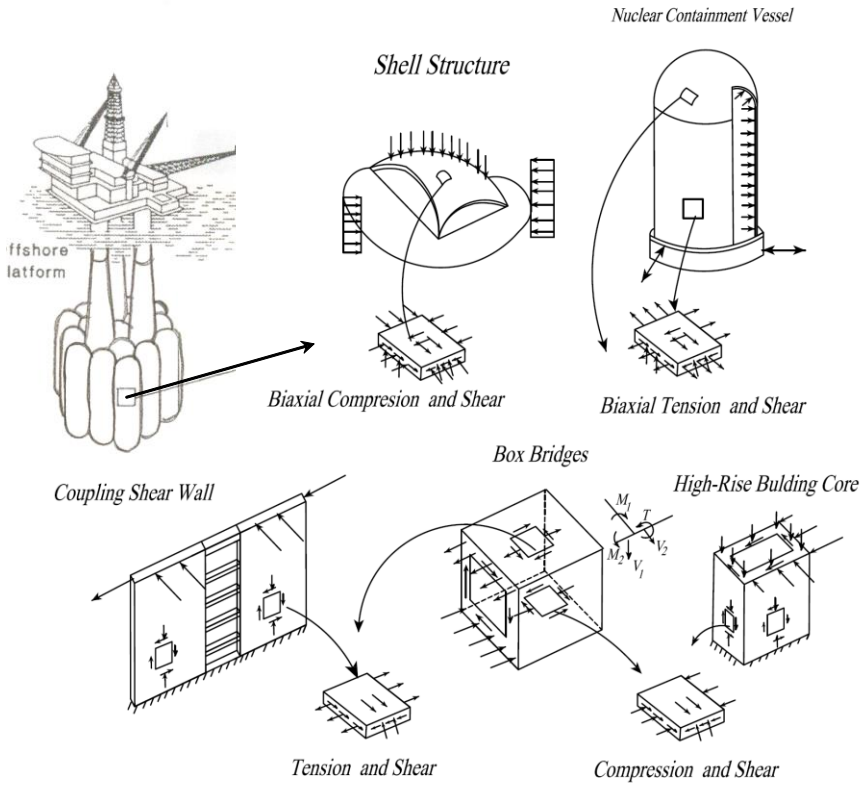

Figure 1 Three dimensional panel elements under various types of stresses

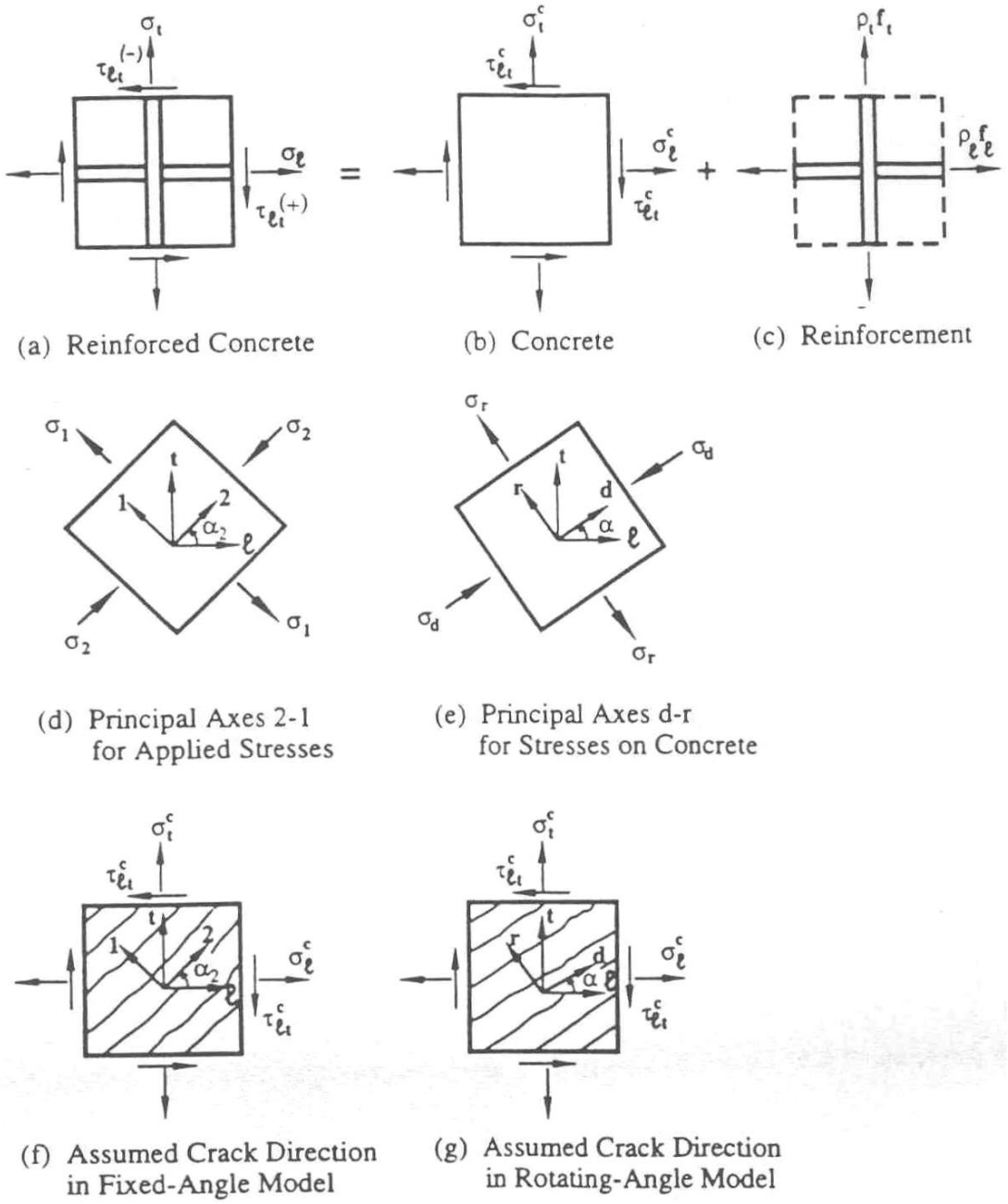

Figure 2 Reinforced concrete membrane elements subjected to in-plane stresses.

Figure 3 3D universal panel tester

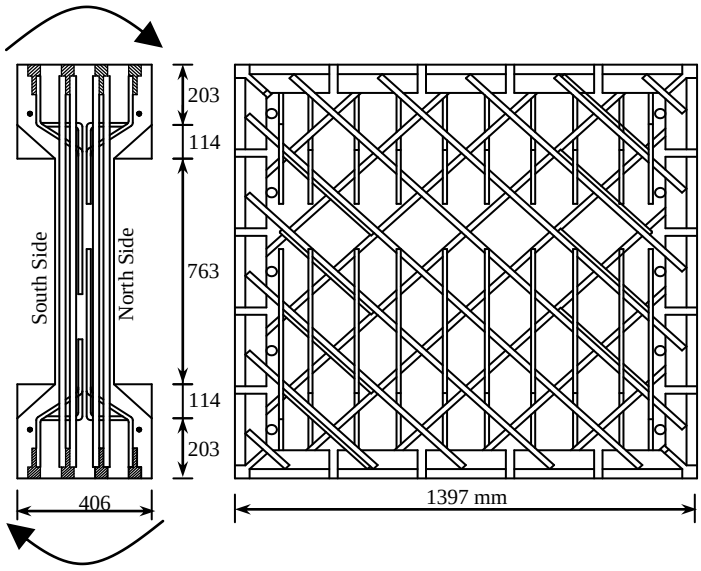

Figure 4 reinforcement layout of panel OP4

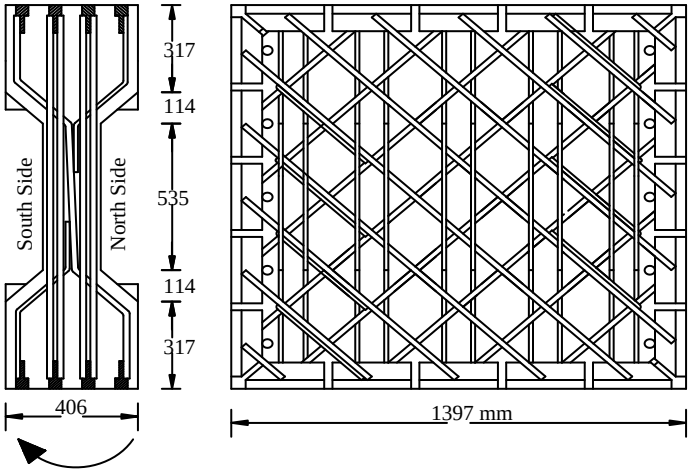

Figure 5 reinforcement layout of panel OP5 and OP6

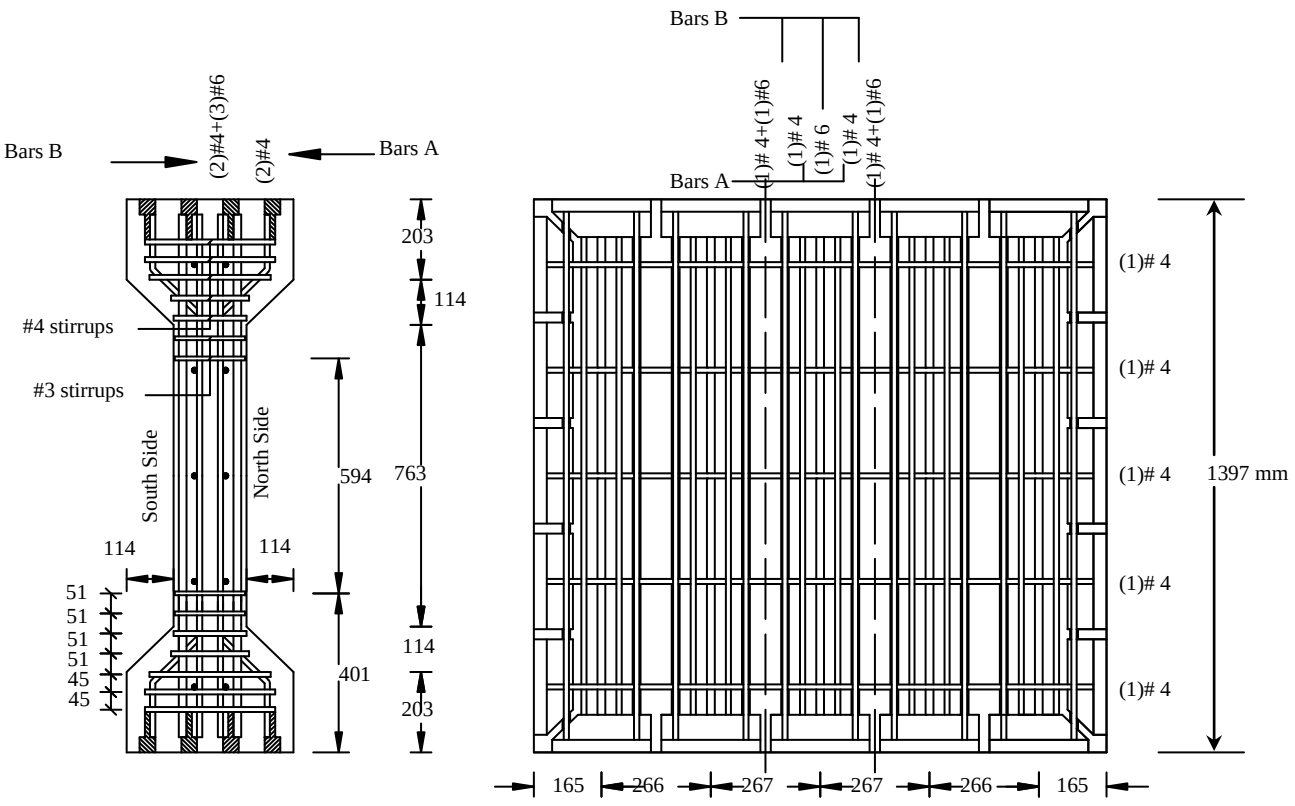

Figure 6 reinforcement layout of panel OPR

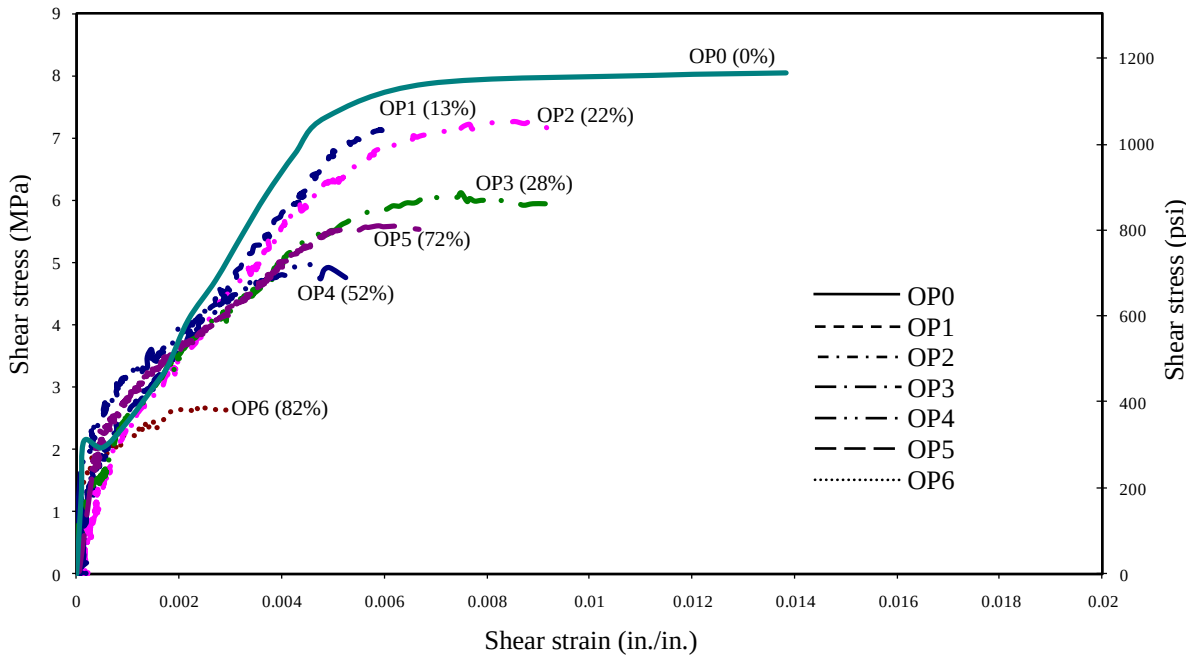

Figure 7 Membrane shear response of the tested specimens

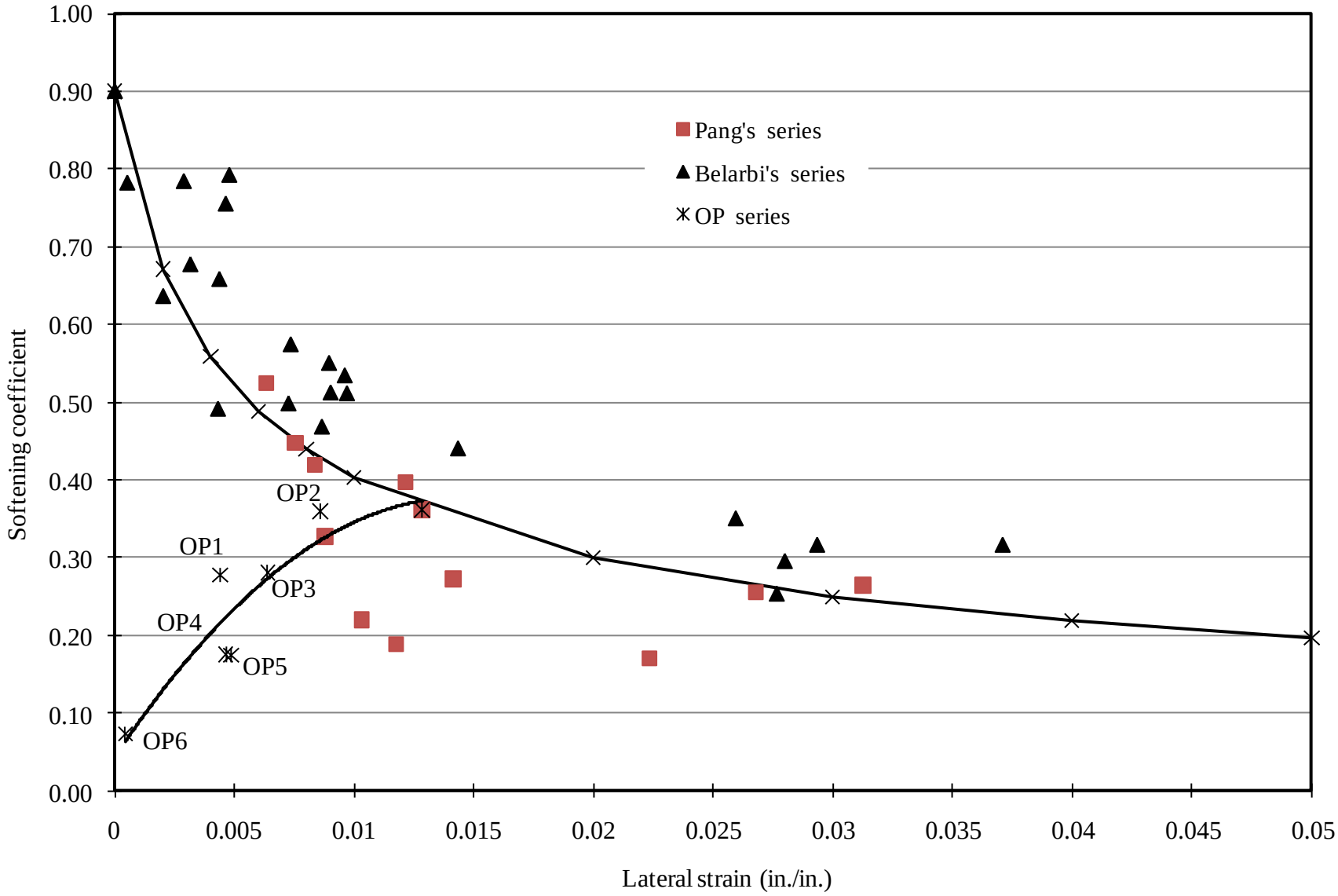

Figure 8 Softening coefficient versus Lateral strain for Belarbi (1991), Pang (1991), and OP panels

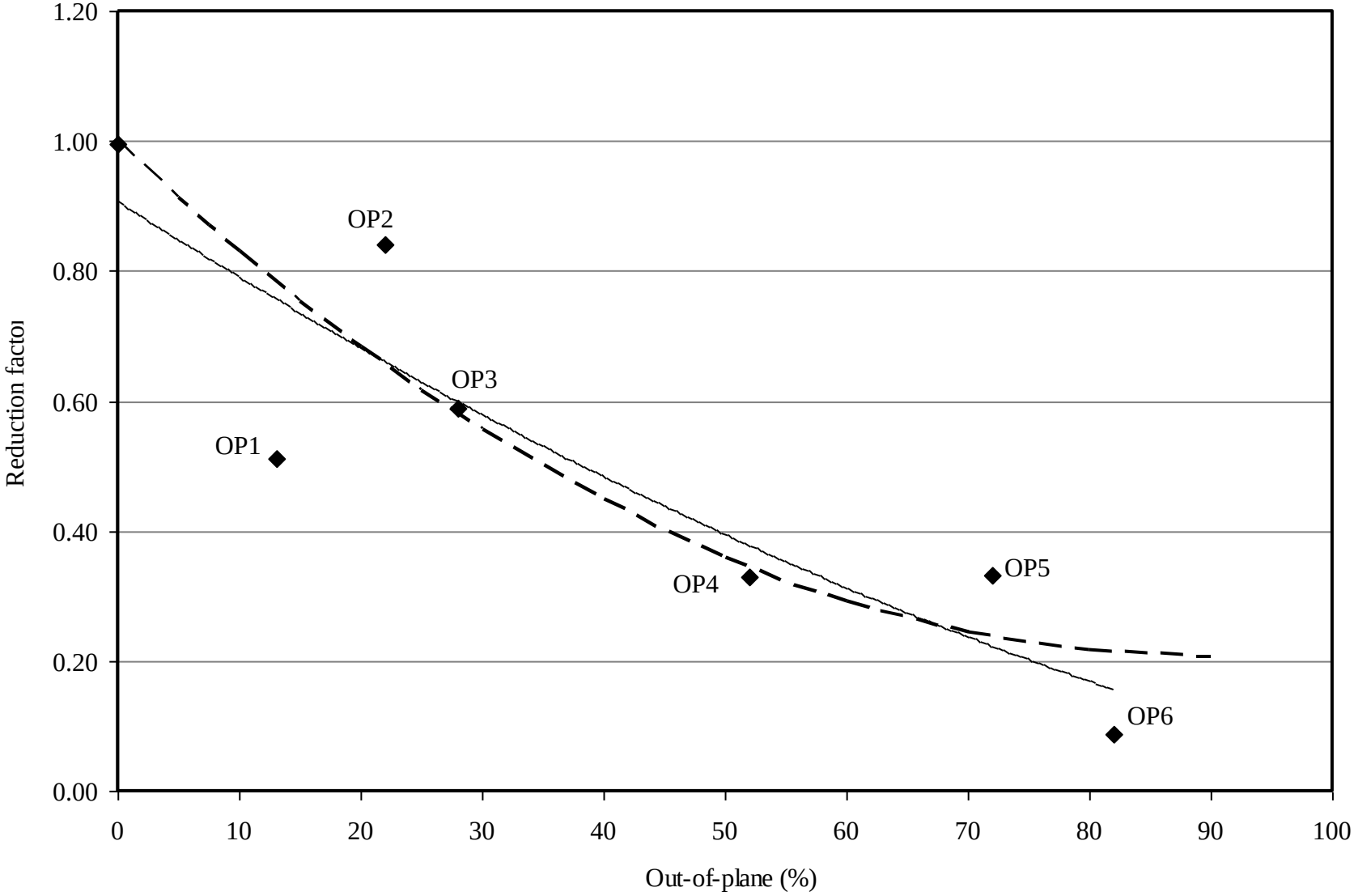

Figure 9 Reduction in the softening coefficient versus percentage of out-of-plane shear

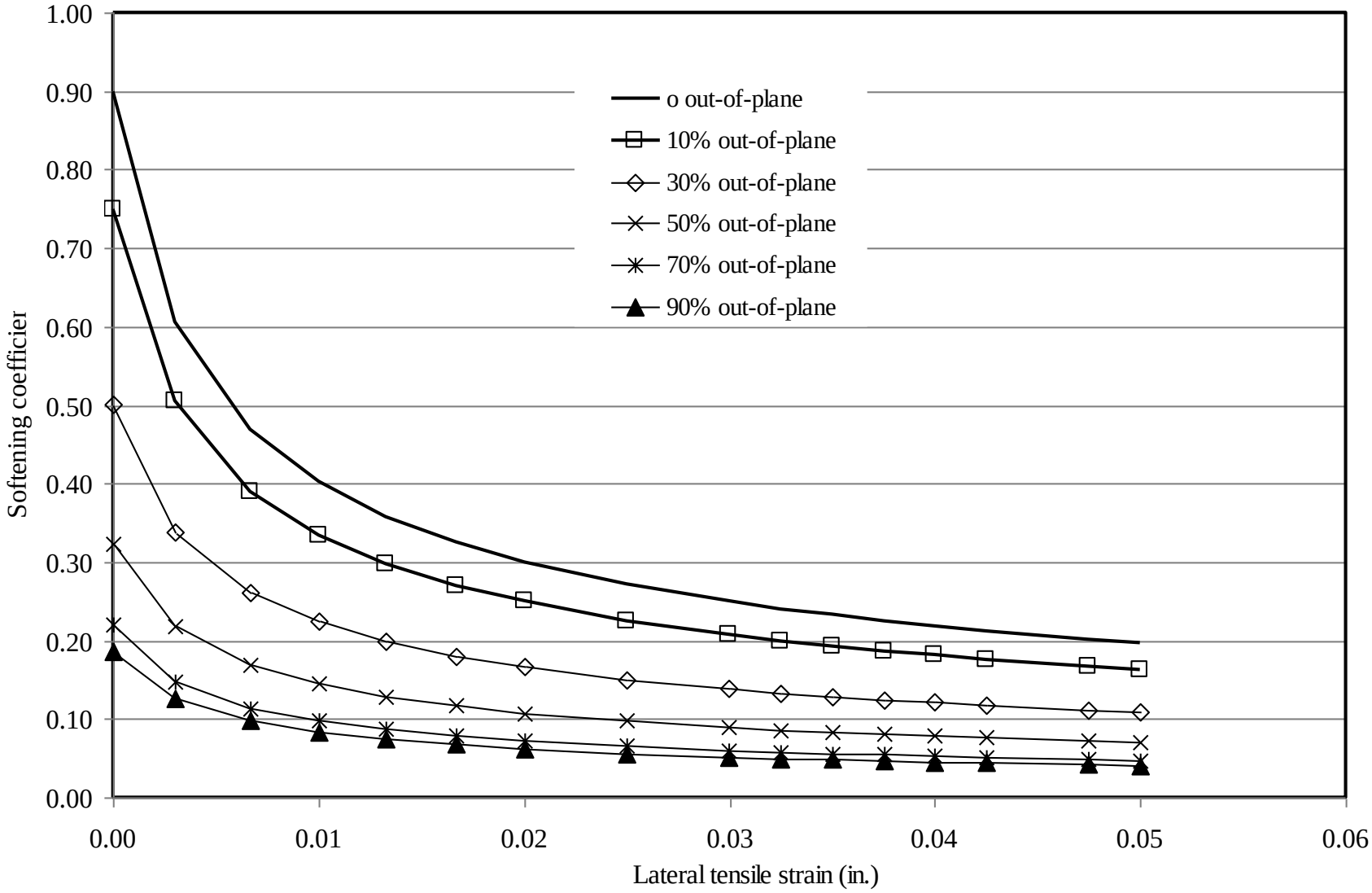

Figure 10 Effect of applying out-of-plane on the softening coefficient

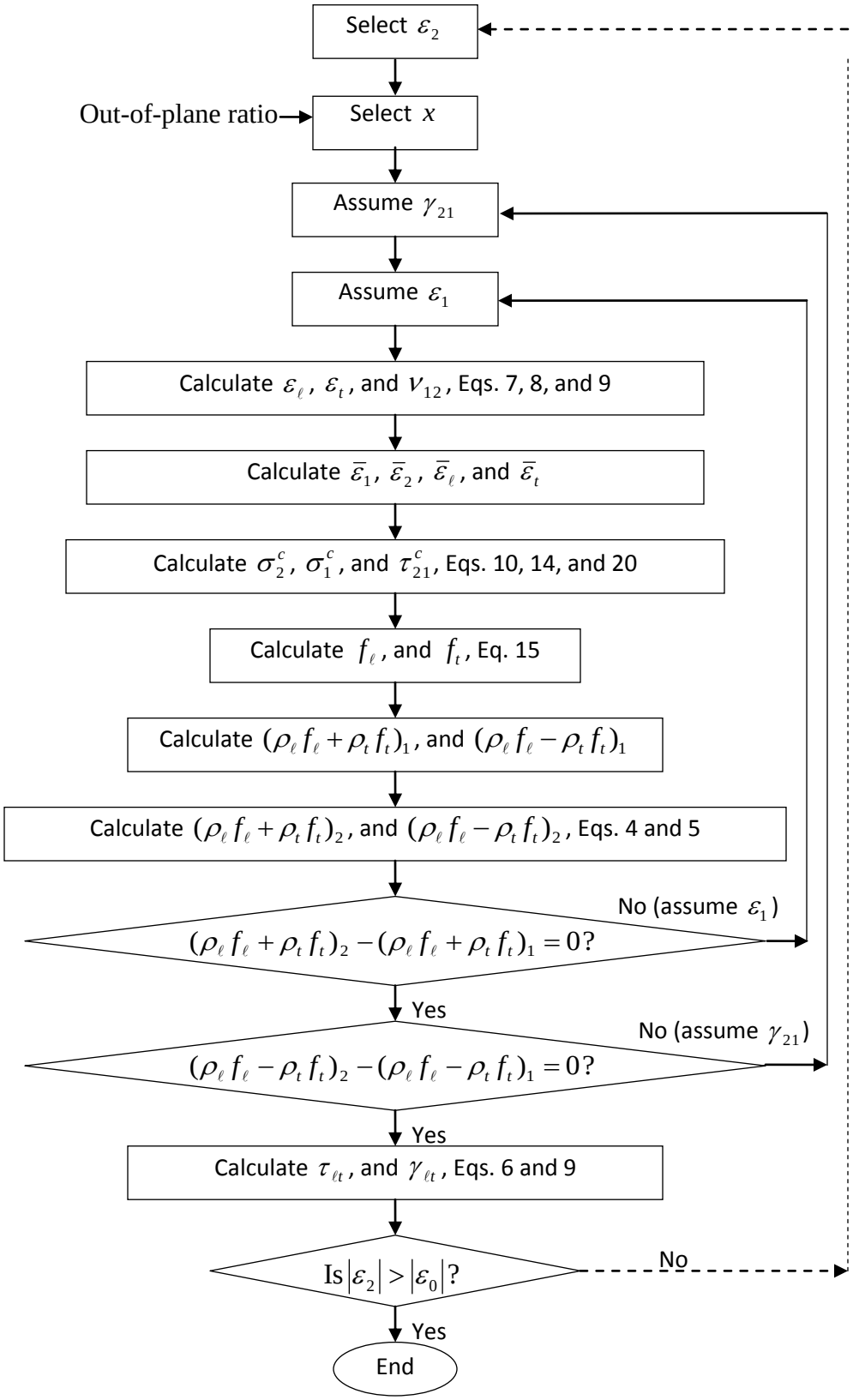

Figure 11 Flow chart of solution procedure for softened membrane model under the effect of out-o-plane shear load

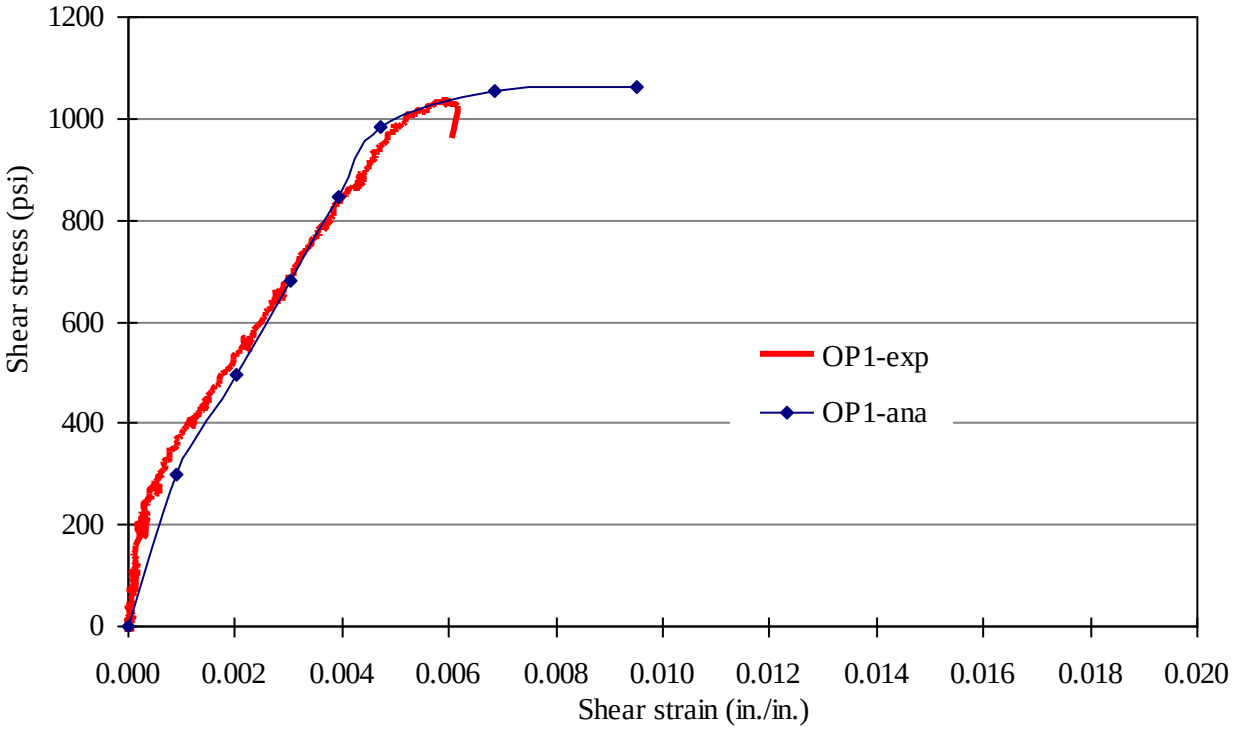

Figure 12 Experimental and analytical in-plane shear stress-strain relationship for OP1

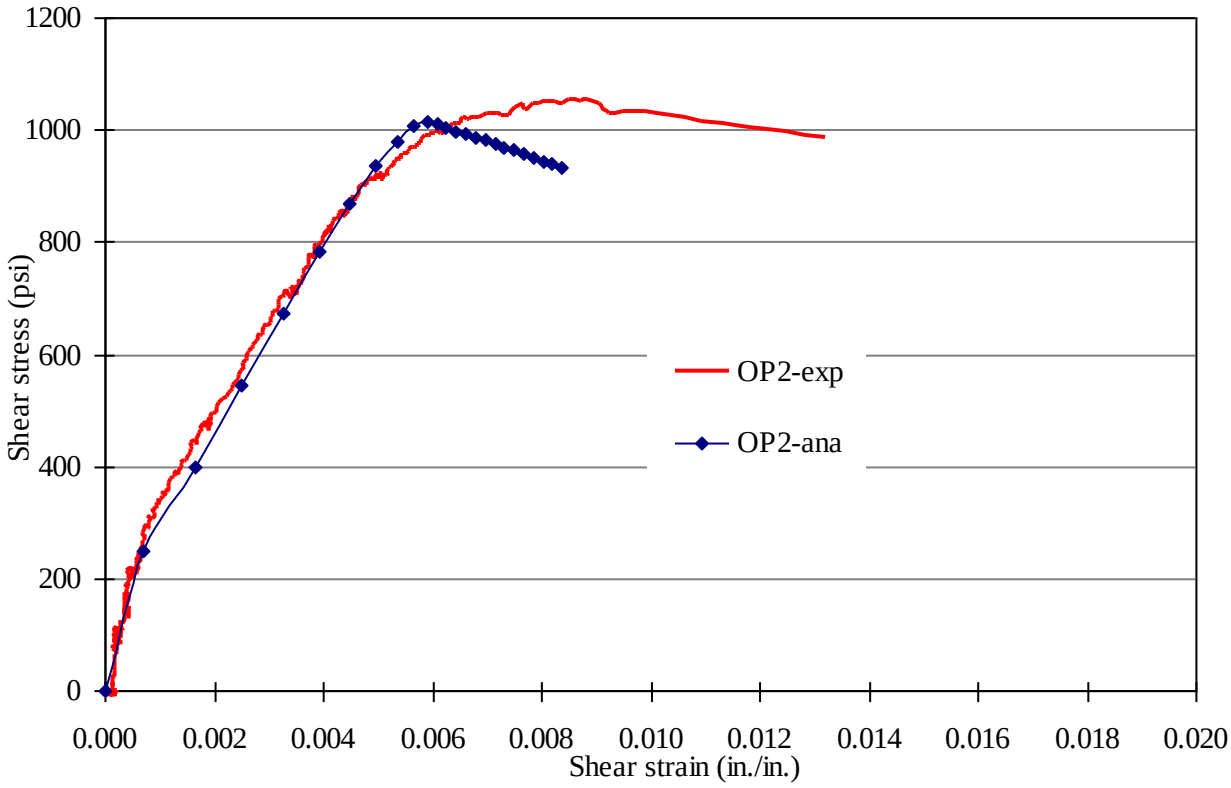

Figure 13 Experimental and analytical in-plane shear stress-strain relationship for OP2

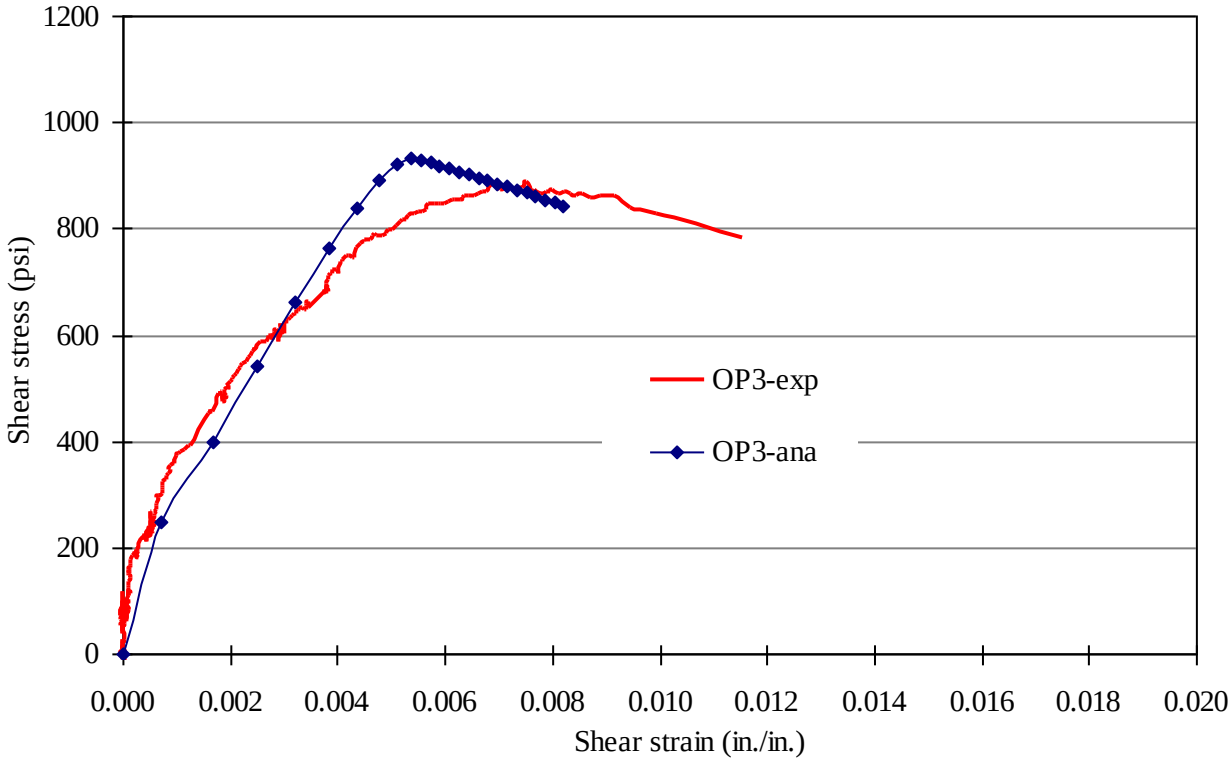

Figure 14 Experimental and analytical in-plane shear stress-strain relationship for OP3

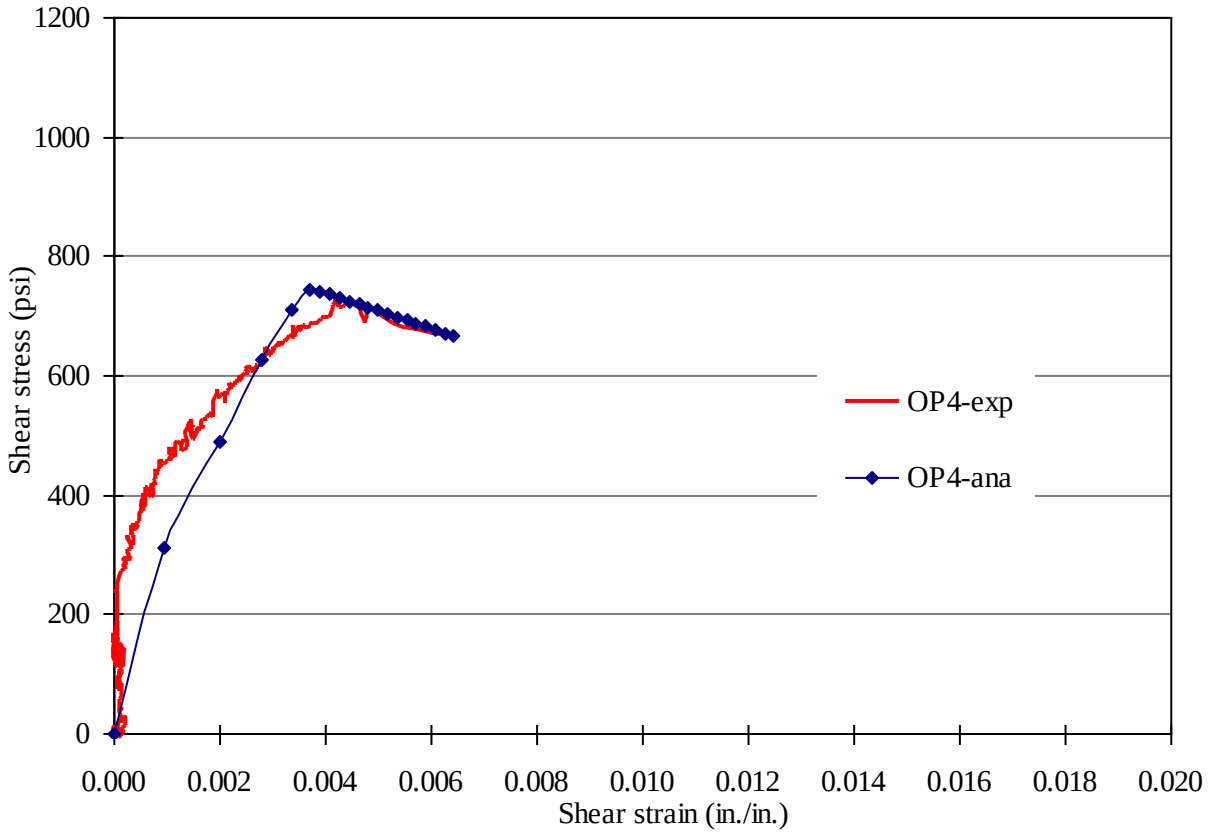

Figure 15 Experimental and analytical in-plane shear stress-strain relationship for OP4

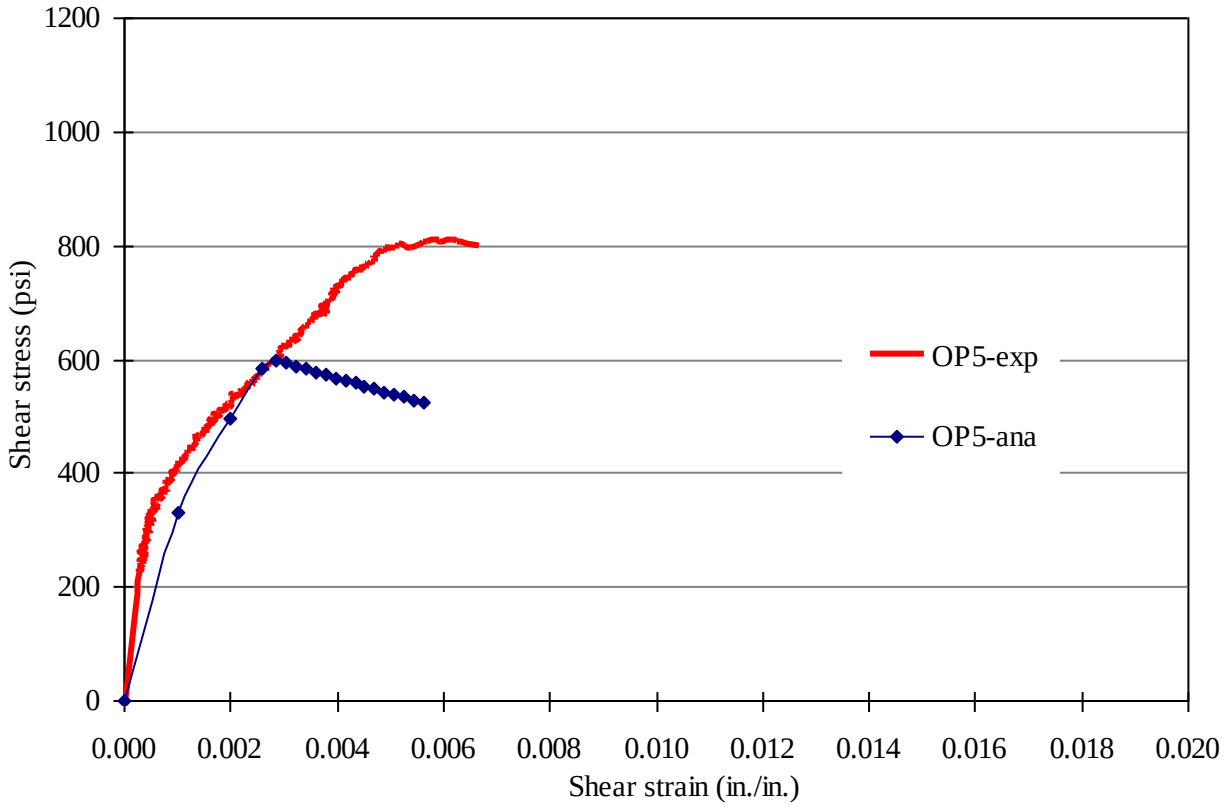

Figure 16 Experimental and analytical in-plane shear stress-strain relationship for OP5

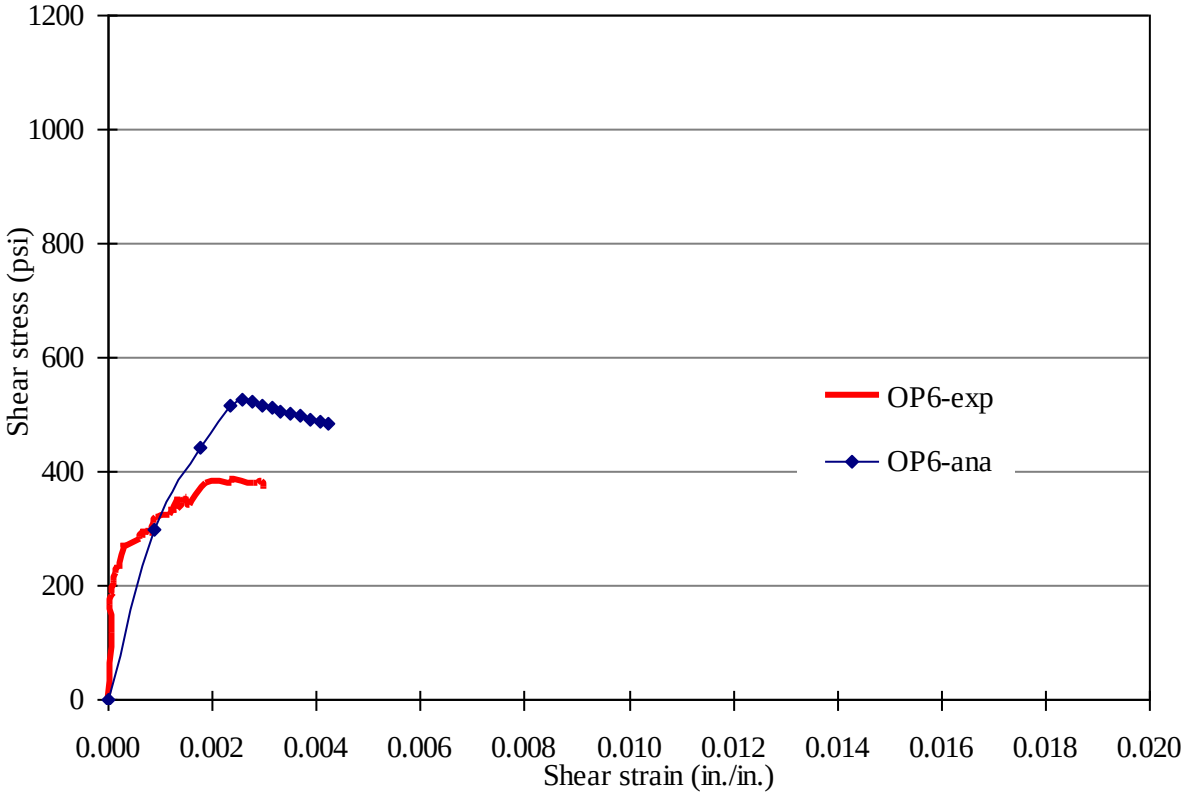

Figure 17 Experimental and analytical in-plane shear stress-strain relationship for OP6

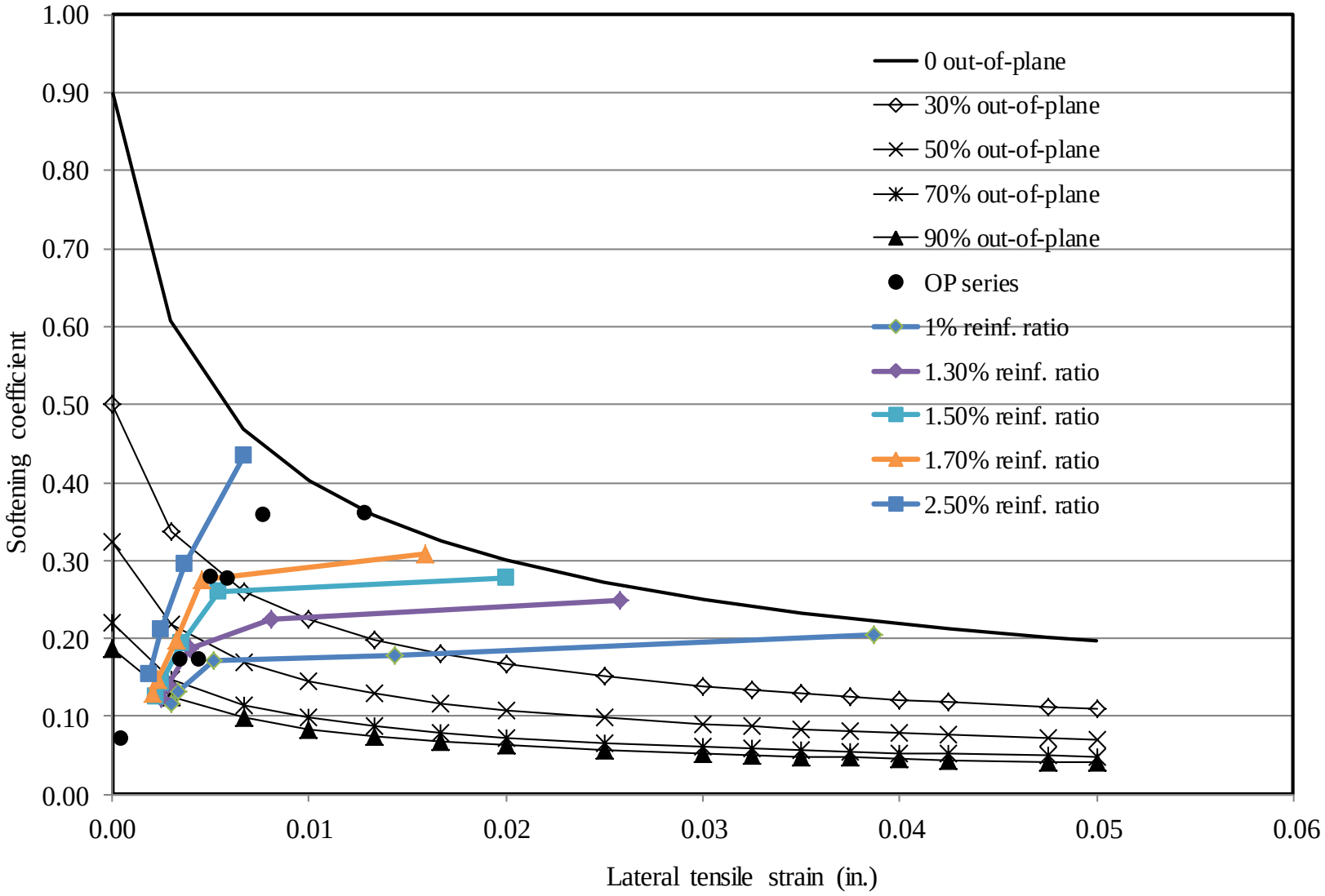

Figure 18 Effect of out-of-plane shear on softening coefficient of membrane elements with different reinforcement ratio

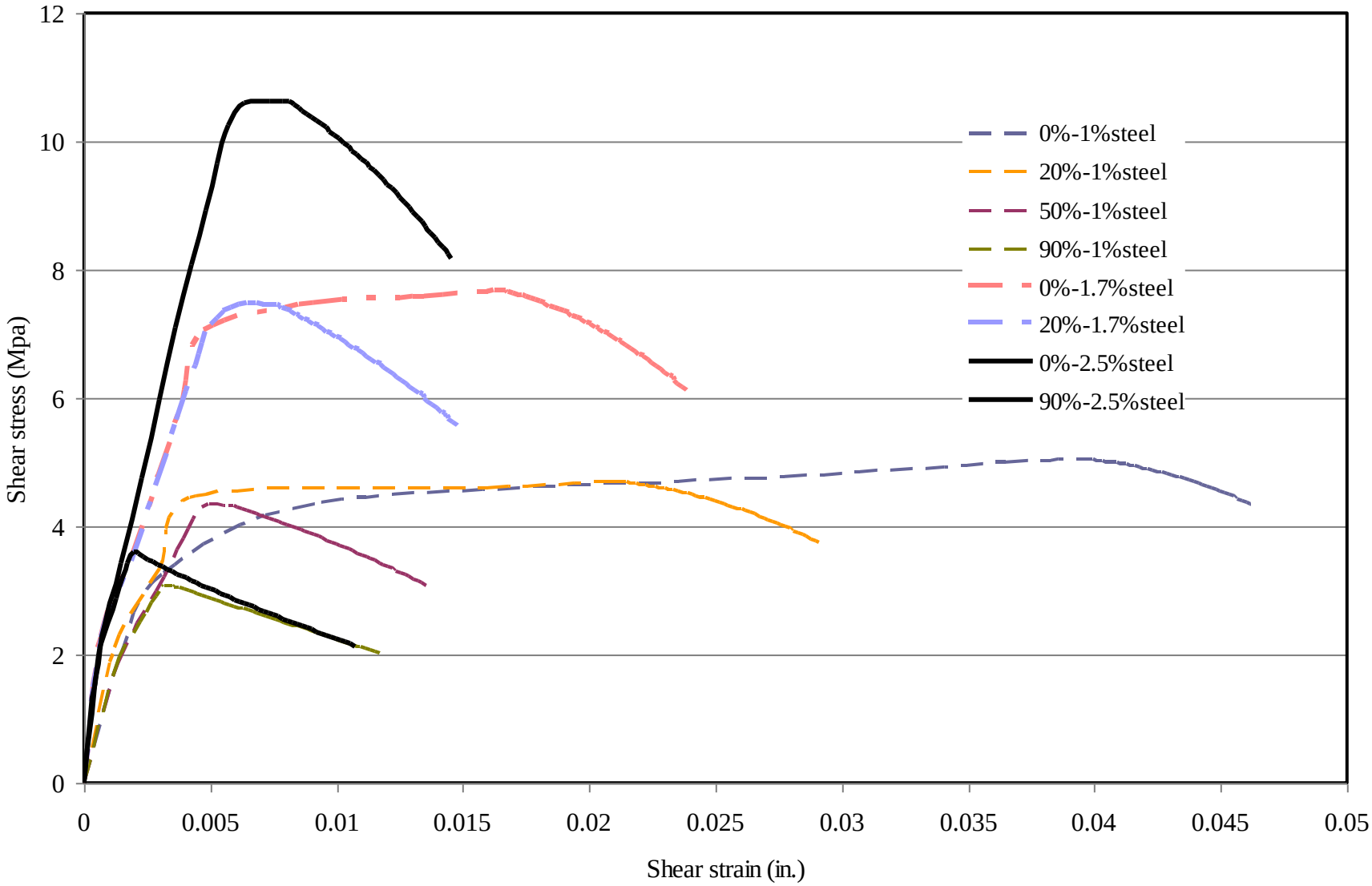

Figure 19 Effect of out-of-plane on shear stress-strain relationship for membrane shear elements with different reinforcement ratios

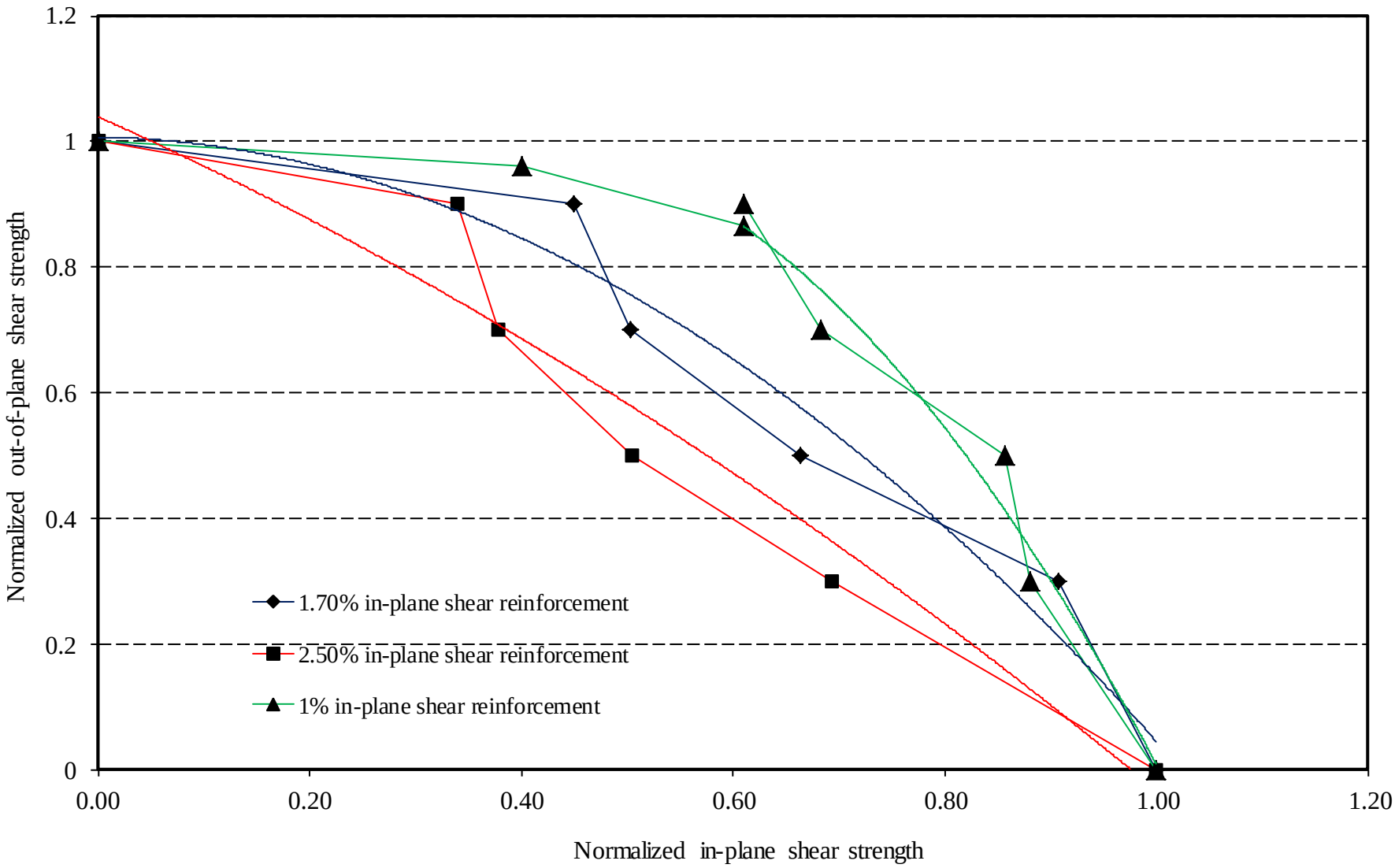

Figure 20 Effect of in-plane shear reinforcement ratio on the in-plane and out-of-plane interaction diagram